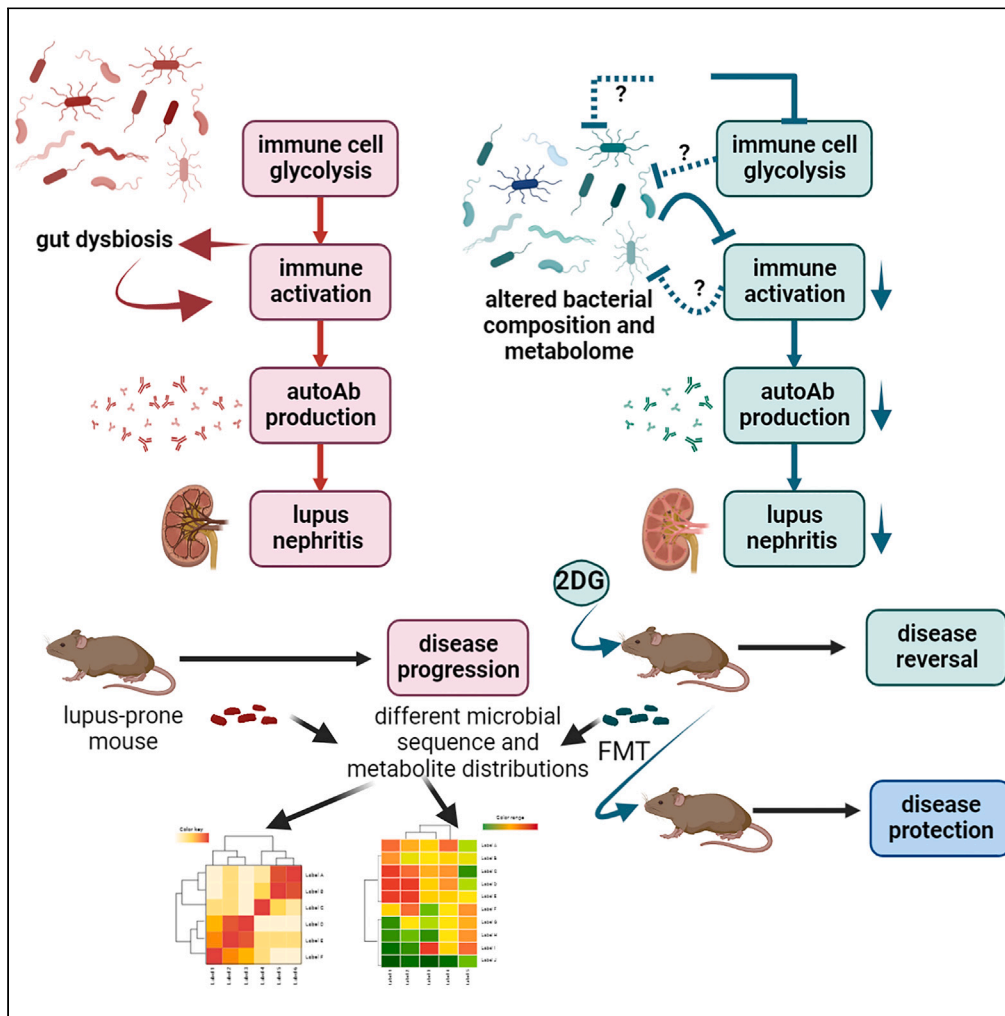## Article

Pharmacologic inhibition of glycolysis prevents the development of lupus by altering the gut microbiome in mice

Ahmed S. Elshikha, Yong Ge, Josephine Brown, ..., William L. Clapp, Mansour Mohamadzadeh, Laurence Morel

morel@uthscsa.edu

Highlights

Gut microbiota from lupus mice transferred autoimmune activation into normal mice

Inhibition of glycolysis with 2DG reversed autoimmune activation in lupus mice

2DG altered the composition and the metabolome of the microbiome of lupus mice

Fecal microbial transfers from 2DG treated mice prevented lupus development

iScience

Article

Pharmacologic inhibition of glycolysis prevents the development of lupus by altering the gut microbiome in mice

Ahmed S. Elshikha,[1,3,4] Yong Ge,[2,3,4] Josephine Brown,[1] Nathalie Kanda,[2] Mojgan Zadeh,[2] Georges Abboud,[1] Seung-Chul Choi,[2] Gregg Silverman,[3] Timothy J. Garrett,[1] William L. Clapp,[1] Mansour Mohamadzadeh,[2,5] and Laurence Morel[2,5,6,*]

SUMMARY

Gut dysbiosis has been associated with lupus pathogenesis, and fecal microbiota transfers (FMT) from lupus-prone mice shown to induce autoimmune activation into healthy mice. The immune cells of lupus patients exhibit an increased glucose metabolism and treatments with 2-deoxy-D-glucose (2DG), a glycolysis inhibitor, are therapeutic in lupus-prone mice. Here, we showed in two models of lupus with different etiologies that 2DG altered the composition of the fecal microbiome and associated metabolites. In both models, FMT from 2DG-treated mice protected lupus-prone mice of the same strain from the development of glomerulonephritis, reduced autoantibody production as well as the activation of CD4+ T cells and myeloid cells as compared to FMT from control mice. Thus, we demonstrated that the protective effect of glucose inhibition in lupus is transferable through the gut microbiota, directly linking alterations in immunometabolism to gut dysbiosis in the hosts.

INTRODUCTION

Systemic lupus erythematosus (SLE) is a chronic autoimmune disorder characterized by pathogenic auto-antibodies, immune-complex formation and multi-organ damage.[1] The underlying pathogenesis of the disease is still poorly understood; however, a combination of genetic and environmental factors has been implicated. Accordingly, growing evidence suggests that gut dysbiosis may contribute to SLE pathogenesis, which has been reported in SLE patients[2–5] and multiple mouse models of the disease (reviewed in[6]). Evidence for causality of intestinal dysbiosis was obtained in several mouse models of lupus. The translocation of *Enterococcus gallinarum* from the gut into host tissues induces an autoimmune response in the TLR7-dependent (NZW x BXSB)F1 (WYaa) mice.[7] The relevance of this finding to lupus pathogenesis was suggested by the presence of elevated titers of antibodies against *E. gallinarium* in SLE patients with antibodies specific to subset of lupus autoantigens.[8] In another TLR7-dependent mouse model of lupus, the translocation of *Lactobacillus reuteri* was pathogenic, and it was reversed by dietary resistant starch and the resulting production bacterial short chain fatty acids (SCFA).[9] Moreover, *Ruminococcus gnavus* blooms have been reported in SLE patients with severe disease,[5] and *R. gnavus* isolated from these patients induces the production of anti-dsDNA autoantibodies in gnotobiotic healthy mice.[10] Finally, fecal microbiome transfers (FMT) from B6.*Sle1.Sle2.Sle3* lupus-prone mice induced autoimmune activation and auto-antibody production in gnotobiotic or antibiotic-treated healthy congenic B6 mice.[11,12] In this latter model, the autoimmune activation was associated with changes in fecal metabolites, especially in the tryptophan pathway, rather than bacterial translocation.[11]

Cellular metabolism is altered in the lupus immune system, especially T cells, and evidence from mouse models and clinical studies support that metabolic inhibitors can ameliorate disease outcomes.[13,14] The combination of 2-deoxyglucose (2DG), a non-metabolizable glucose analog that inhibits the first step of glycolysis, and metformin, an inhibitor of complex 1 in the mitochondrial electron transport chain, reduced the metabolism and the expansion of activated CD4+ T cells, prevented the production of autoantibodies, and reversed disease in multiple mouse models.[15] Furthermore, we showed that the inhibition of glycolysis by 2DG alone reversed the production of autoantibodies and expansion of follicular helper T (Tfh) cells as

[1]Department of Pathology, Immunology, and Laboratory Medicine, University of Florida, Gainesville, FL 32610, USA

[2]Department of Microbiology, Immunology, and Molecular Genetics, University of Texas Health, San Antonio, TX 78229, USA

[3]The Laboratory of B Cell Immunobiology and the Division of Rheumatology, NYU School of Medicine, New York, NY 10016, USA

[4]These authors contributed equally

[5]Senior author

[6]Lead contact

*Correspondence: morel@uthscsa.edu

https://doi.org/10.1016/j.isci.2023.107122

well as germinal center (GC) B cells, without impairing the response to foreign antigens in lupus-prone mice.[16] Metformin by itself showed only modest effects on autoimmune pathogenesis,[15,17] although it reduced the response of human CD4^{+} T cells to type I interferon,[18] as well as the occurrence of flares in SLE patients.[19]

Metformin has been shown to drastically modify the gut microbiome of diet-induced obese mice, most notably with a bloom of mucin-degrading *Akkermansia* populations.[20] Oral administration of *Akkermansia* to mice fed with a high fat diet largely reproduced the anti-diabetic therapeutic effect of metformin.[20] Metformin also alters the gut microbiome of patients with type 2 diabetes,[21] including an expansion of SCFA-producing bacterial populations, which have been shown to reduce blood sugar levels by inducing intestinal neoglucogenesis. These results have been interpreted as the therapeutic effect of metformin being at least in part mediated through changes in the microbiome. Based on this model, we postulated that the therapeutic effects of 2DG in lupus could also be mediated through a modulation of the dysbiotic microbiome. To our knowledge, the effect of 2DG or glycolysis inhibition in general has not been investigated on the gut microbiome. We tested this hypothesis in two models: the (NZB x NZW)F1 (BWF1) female mice, a classical model of lupus that presents gut dysbiosis[3] as well as a beneficial response to 2DG,[15,16] and WYaa mice, a male model of lupus with a different etiology,[22] as well as a translocation mediated involvement of gut pathobionts.[7] After establishing that 2DG also has therapeutic effects in WYaa mice, we showed that 2DG profoundly altered the composition of the fecal microbiome and metabolome in both strains. Furthermore, we showed that these changes were functional since serial FMT from 2DG-treated mice prevented disease development in the two models. Therefore, the protective effect of glycolysis inhibition in lupus is mediated at least in part through changes in the intestinal microbiota.

RESULTS

2DG altered the gut microbiota and metabolome of BWF1 mice

In lupus-prone mice, treatment with 2DG combined with metformin reversed disease,[15] and 2DG alone reversed the expansion of Tfh and GC B cells, as well as the production of anti-dsDNA IgG.[16] To elucidate whether inhibiting glycolysis with 2DG alters the gut microbiota, we treated BWF1 mice with 2DG starting at age 20 weeks, an early stage of disease onset whereby these mice produce autoantibodies but have not yet developed renal pathology. The treatment lasted for 4 weeks, then was reinitiated at age 36 weeks when the production of anti-dsDNA IgG was detected again. 2DG treatment continued until mice were euthanized at age 46 weeks. Age-matched untreated mice were also euthanized when they presented heavy proteinuria. As expected, 2DG prevented early death as well as the development of renal pathology as assessed by proteinuria, and glomerulonephritis (GN) score (Figures S1A–S1C). 2DG reduced complement C3, IgG2a immune complex deposition, infiltration of F4/80^{+} macrophages, and CD3^{+} T cells in the kidneys when compared to controls (Figures S1D–S1H). 2DG also reduced the production of anti-nuclear antibodies (ANA) and anti-dsDNA IgG (Figures S1I and S1J).

Next, we analyzed the fecal microbial composition of BWF1 mice before (age 20 weeks), and after 2DG treatment (age 46 weeks). While there was no difference in alpha-diversity (Figure 1A), the 2DG treatment significantly shaped the gut microbiota composition, resulting in distinct bacterial community clusters (Figure 1B). The microbiota of control mice shifted over time likely because of disease progression; however, this shift was restricted by 2DG, as shown by reduced unweighted UniFrac distances (Figure 1C). Compositional analysis demonstrated that 2DG treatment did not skew the Firmicutes to Bacteroidetes ratio (Figure 1D), although it was found to be one of the most consistent features of lupus fecal microbiome.[23] However, a bacterial class, Mollicutes, as well as several genera, Anaeroplasma, Lactobacillus, RF39 and Sutterella, all of which have been reported to be less abundant in SLE patients compared to healthy controls,[24,25] were sustained in BWF1 mice treated with 2DG, compared to controls (Figures 1E and 1F). In addition, the level of *Parabacteroides distasonis*, possessing the ability to mitigate intestinal inflammation,[26] was also enriched in 2DG-treated mice (Figure 1F). In contrast, the abundance of Desulfovibrio, AF12, *Bacteroides acidifaciens*, and Bacteroidales, which were elevated in the TLR7-dependent SLE mouse model9, as well as Turicibacter, that was enriched in B6.*Sle1.Sle2.Sle3* lupus-prone mice compared to B6 mice,[11] were all decreased in BWF1 mice after 2DG treatment (Figure 1F). Overall, these results indicate that 2DG treatment modifies the gut microbiota during disease development in BWF1 mice.

Analyzing fecal microbiota-associated metabolites of 2DG-treated mice compared to controls at age 46 weeks demonstrated distinct profiles by both positive and negative ionizations and greatly reduced
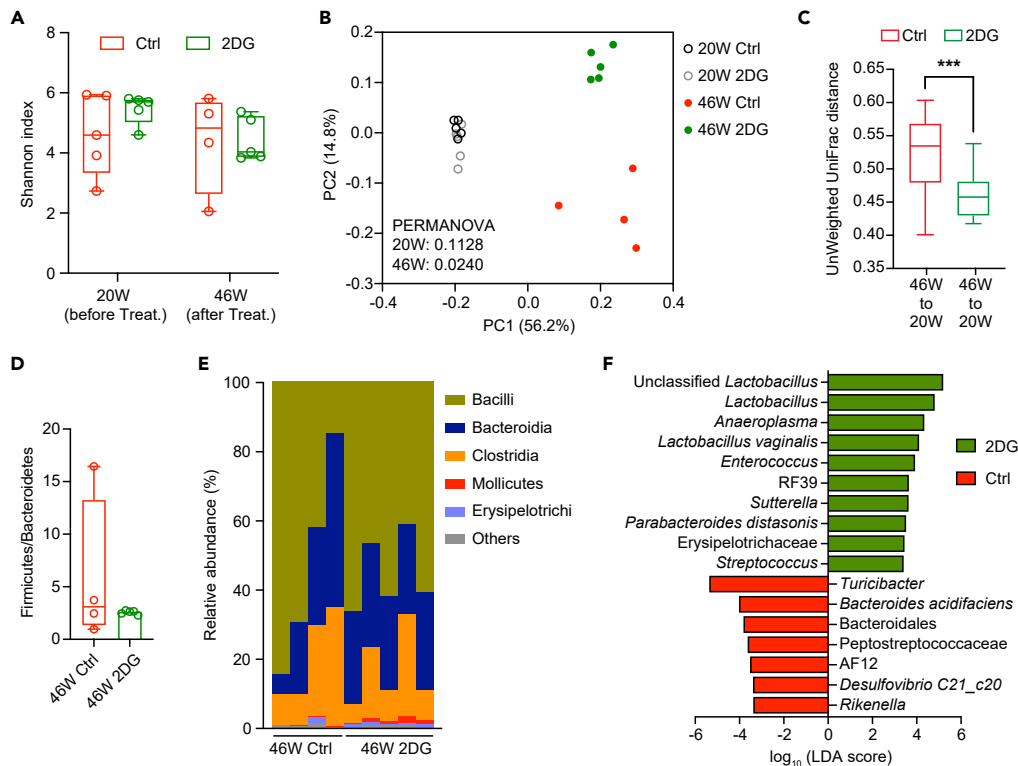
Figure 1. 2DG treatment impacted gut microbiota composition in BWF1 mice

16S rRNA sequencing of the feces collected from BWF1 mice before (age 20 weeks) and after 2DG treatment (age 46 weeks).

(A) Shannon index measuring bacterial diversity.

(B) Unweighted Unifrac principal coordinate analysis (PCoA) plot showing the bacterial community structure. The PERMANOVA q values are indicated for the two time-points.

(C) Unweighted UniFrac distances between 20 and 46 weeks showing an increased similarity in BWF1 mice by 2DG.

(D) Firmicutes/Bacteroidetes ratio at age 46 weeks.

(E) Bacterial class abundance at age 46 weeks. Each bar represents a mouse.

(F) Linear discriminant analysis effect size (LEfSe) plot showing differentiating taxa (species level) between 2DG-treated mice and controls at the age of 46 weeks (n = 4–5 per group); ***p < 0.001; Mann–Whitney U test (C). See also Figure S1.

interindividual variability (Figure 2A). Metabolic pathways related to vitamins, carbohydrates (e.g., the pentose phosphate pathway, sialic acid, and N-glycan), lysine and purine metabolisms were influenced by 2DG treatment (Figure 2B). Accordingly, 2DG-treated mice exhibited enriched cofactors, including vitamin B6 (pyridoxine, pyridoxine 5′-phosphate, pyridoxal), and vitamin C (ascorbic acid), amino acids (e.g., lysine, aspartate, asparagine), nucleobases (e.g., adenine, cytosine, guanine), and carbohydrates (e.g., galactose, UDP-galactose, 3-ketolactose, deoxyribose, glucosamine), potentially supporting gut microbial growth (Figure 2C). Notably, a panel of compounds with antioxidant properties, including lipoamide, putrescine, salicyluric acid, gluconolactone, mevalonolactone and isopentenyl diphosphate, were also significantly enriched by the 2DG treatment, while the oxidative stress markers such as ethylmalonic acid, allantoin, as well as associated metabolites allantoate and alloxan were decreased (Figure 2C). Consistent with increased abundance of *Lactobacillus* (Figure 1F), lactate was correspondingly enhanced in the fecal samples of 2DG-treated mice (Figure 2C). In addition, metabolites potentially modulating intestinal epithelial mitochondrial function, including acetylcholine, carnitine, and acetylcarnitine, were also observed at significantly higher levels in 2DG-treated mice compared to controls (Figure 2C). Finally, we have previously shown that an altered tryptophan metabolism was associated with autoimmune pathogenesis in B6.*Sle1.Sle2.Sle3* mice,[11] which is largely caused by an enhanced fecal tryptophan catabolism.[27] Here, 2DG increased the abundance of both fecal tryptophan and kynurenic acid, potentially rescuing this imbalance. Together, these results suggest a critical role of 2DG in functionally modulating gut microbiota composition and metabolite output in BWF1 mice.
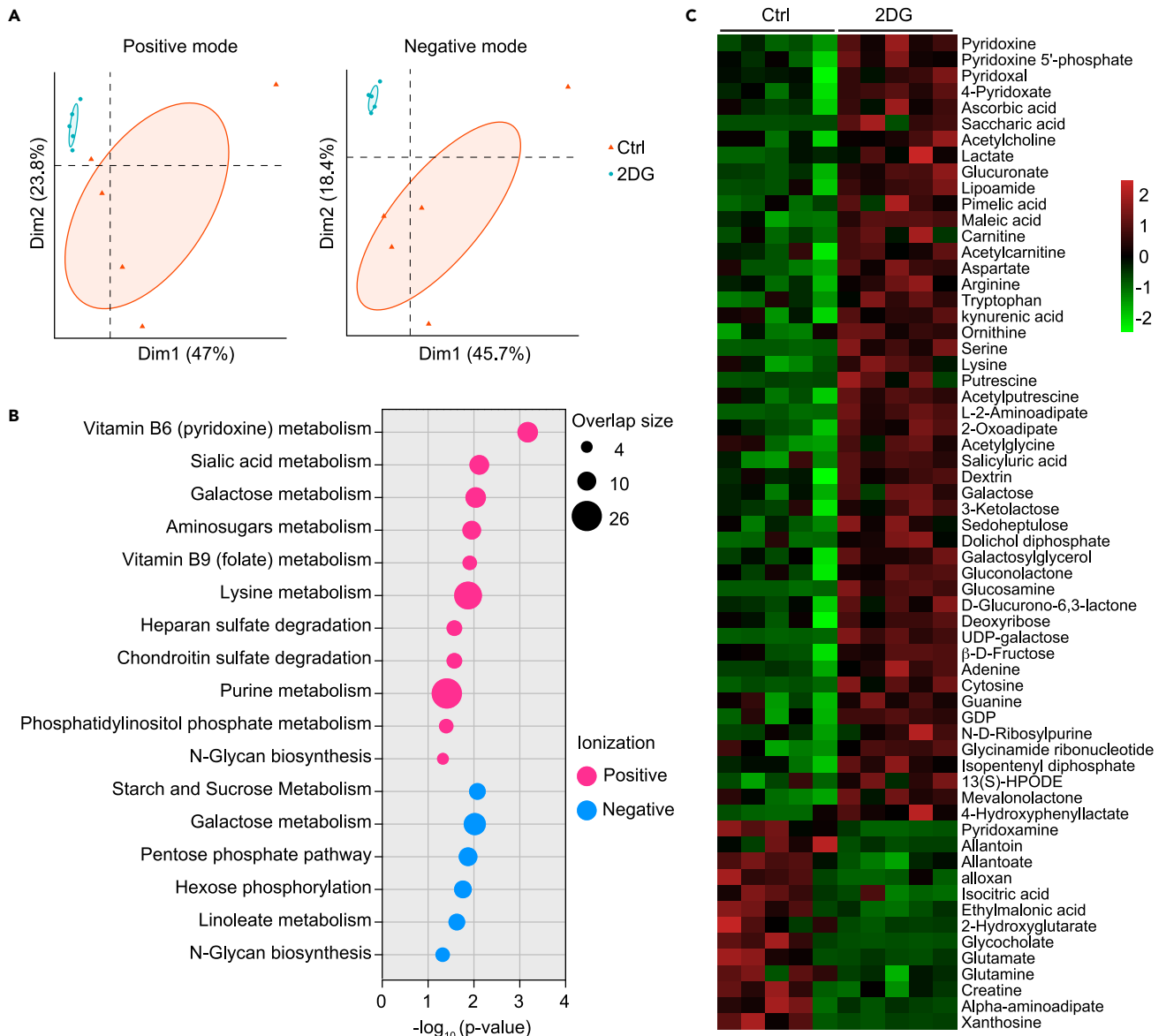
Figure 2. 2DG treatment altered gut microbiota-associated metabolites in BWF1 mice

(A) Principal component analysis (PCA) plots of metabolite features identified by positive and negative ionization in feces collected from 2DG-treated versus untreated BWF1 mice (n = 5 per group).

(B) Metabolic pathway analysis of metabolites with significantly differing counts between 2DG-treated and control mice. The overlapped size indicates the number of significant metabolic features mapped to corresponding pathways.

(C) Heatmap showing differentially enriched metabolites. See also Figure S1.

Fecal microbiota transfers from 2DG-treated mice protected BWF1 mice from autoimmune pathology

The protective potential of the gut microbiota from 2DG-treated mice was assessed by fecal microbiota transfers (FMT) into pre-autoimmune 8-week-old BWF1 mice whose microbiota had been previously depleted by a 2-week treatment with an antibiotic cocktail. FMT from untreated mice (Ctrl-FMT) as well as PBS gavages in antibiotic-pretreated 8-week-old recipients were used as controls (Figure S2A). FMT from 2DG-treated mice (2DG-FMT) reduced renal pathology in recipients as assessed by proteinuria and GN score compared to the recipients of Ctrl-FMT and PBS (Figures 3A–3C). The glomeruli of all PBS-treated and Ctrl-FMT mice showed prominent mesangial and endocapillary hyperplasia with classical
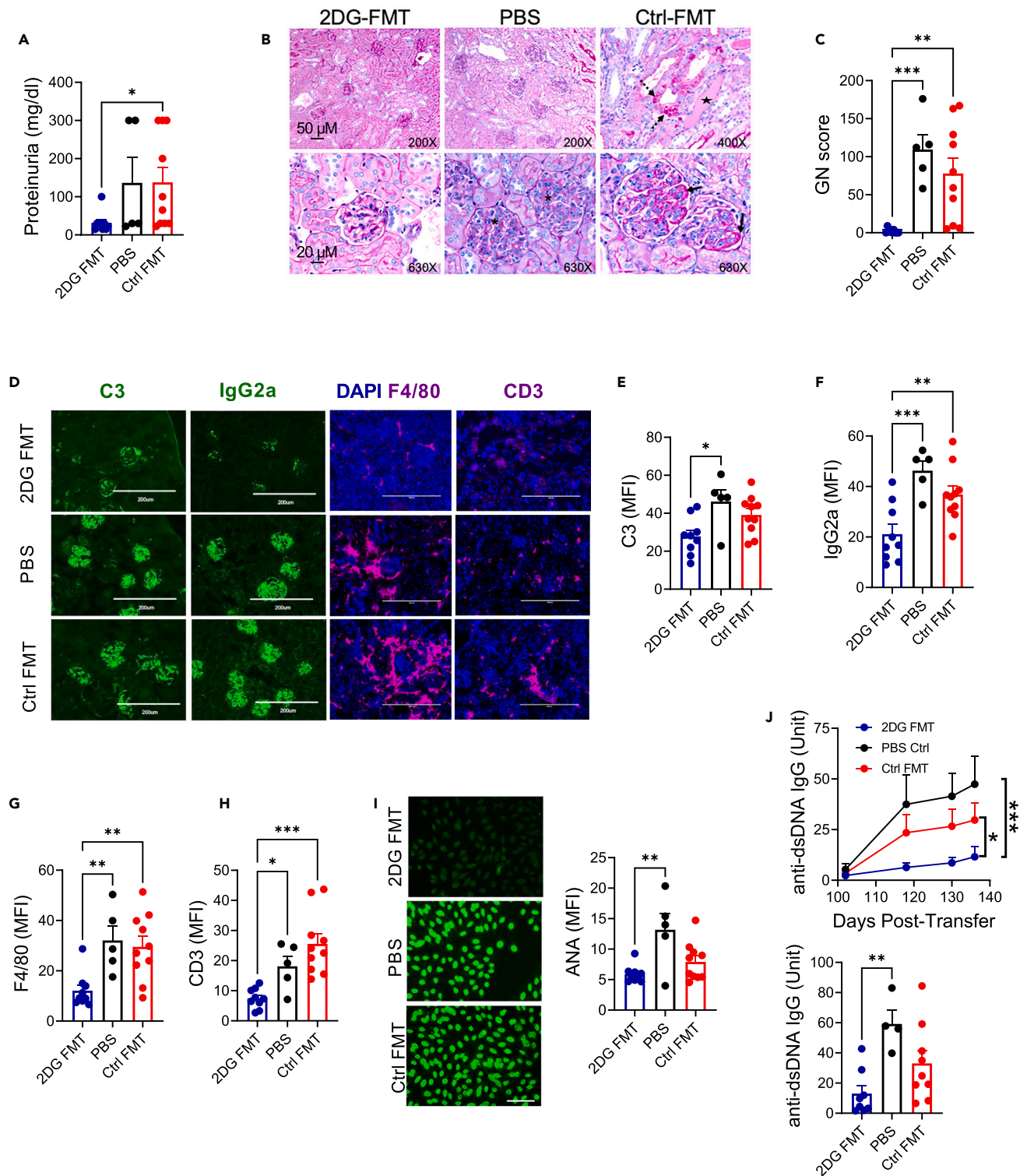
Figure 3. FMT from 2DG-treated mice reduced renal pathology and autoantibody production in BWF1 mice

Antibiotic-pretreated 8-week-old BWF1 mice received 2DG-FMT, Ctrl-FMT or PBS for 20 weeks.

(A) Terminal proteinuria.

Figure 3. *Continued*

(B) Representative PAS-stained kidney sections at medium (top, scale bar 50 μM) and high (bottom, scale bar 20 μM) magnifications as indicated. The * symbols indicate endocapillary hypercellularity, the star symbol shows a cast, dashed arrows show protein droplets in dilated proximal tubules and plain arrows show "wire-loop" peripheral hyaline deposits.

(C) GN scores.

(D) Representative images of C3, IgG2a immune complex deposition, F4/80+ macrophages and CD3+ T cells in glomeruli. Nuclei were stained with DAPI (20x, scale bars: 100 μM).

(E–H) Quantification of C3 and IgG2a deposition, and F4/80+ and CD3+ cells (MFI: mean fluorescence intensity).

(I) Representative images of terminal serum ANA (20x, scale bar 100 μM) and ANA intensity quantification.

(J) Time course analysis (two-way ANOVA) and terminal values of serum anti-dsDNA IgG. Each symbol represents a mouse, bars show means ± SEM. n = 4–10 mice per group. One-way ANOVA with Dunnett's multiple comparison tests unless indicated, *p < 0.05, **p < 0.01 and ***p < 0.001. See also Figure S2.

"wire-loop" lesions, and some of these mice also presented mesangial hyaline deposits. In addition, some kidneys showed casts, proximal tubule dilatation, and protein resorption droplets, indicating a severe renal injury. In contrast, all 2DG-FMT mice showed a normal renal cortex with very few hypercellular glomeruli, and no hyaline deposits. Kidneys of 2DG-FMT mice also showed reduced amounts of C3 and IgG2a deposition, as well as reduced F4/80+ macrophage and CD3+ T cell infiltration (Figures 3D–3H). 2DG-FMT mice produced less ANA and anti-dsDNA IgG as compared to PBS-treated controls, and there was a similar trend for Ctrl-FMT mice (Figures 3I–3J). Together, these results show that FMT from 2DG treated mice reduced the development of renal pathology and the production of autoantibodies.

Next, we evaluated the impact of 2DG-FMT on immune activation. After 20 weeks of transfer, 2DG-FMT mice showed lower splenocyte numbers (Figure 4A) as well as reduced CD4+ T cell activation represented by the frequency of CD69+ T cells (Figure 4B) compared to both Ctrl-FMT and PBS. In addition, the frequency of IFN-γ+ CD4+ T cells was diminished in 2DG-FMT compared to Ctrl-FMT mice (Figure 4C). The frequencies of IL-17A+, effector memory (Tem), follicular helper (Tfh) CD4+ T cells, and the Tfh to follicular regulatory (Tfr) T cell ratio were reduced compared to PBS controls (Figures 4D–4G). The values obtained from Ctrl-FMT for these parameters were intermediate between the 2DG-FMT and PBS control groups (Figures 4D–4G). Intriguingly, a similar reduction was obtained for Foxp3+ regulatory CD4+ T cells (Figure 4H). 2DG-FMT exerted no effect on the frequency of GC B cells, but it reduced the frequency of plasma cells (PC) compared to PBS controls (Figures 4I and 4J). Furthermore, the frequency of CD11c+ MHC-II+ conventional dendritic cells (cDC) was reduced in 2DG-FMT compared to both Ctrl-FMT and PBS mice (Figure 4K). Finally, as compared to control mice, 2DG-FMT decreased the frequency of inflammatory plasmacytoid DCs (ipDCs), a subset of B220- pDCs secreting high amounts of type I interferon (IFN), and thus play a detrimental role in lupus manifestation[28] (Figure 4L). Similar effects were observed in the mLN where frequencies of activated CD69+ T cells, Tem cells, Tfh cells, and the ratio of Tfh to Tfr cells were reduced in 2DG-FMT mice compared to both groups of control mice (Figures S3A–S3D). Consistent with observations in the spleen (Figure 4), there was no difference in the frequency of GC B cells but the frequencies of PCs, cDC, and ipDCs were reduced in 2DG-FMT mice (Figures S3E–S3H). These results indicate that the fecal microbiota from 2DG-treated BWF1 mice decreased autoimmune activation of CD4+ T cells and DCs as well as plasma cell production in younger mice from the same strain compared to controls. The transfer of microbiota from untreated BWF1 mice demonstrated by itself a mitigating effect with intermediate activation values between 2DG FMT and PBS controls.

To elucidate whether the immunological phenotypes of 2DG-FMT mice are associated with a protective role of gut microbiome in recipient mice, the fecal microbiota of 2DG-FMT, Ctrl-FMT and PBS control mice was analyzed at age 28 weeks (terminal collection) and compared to 2DG and control donors (Figure S2A). Albeit no difference in alpha-diversity was observed between 2DG-FMT and Ctrl-FMT mice (Figure 5A), these groups of mice displayed distinct bacterial community structures, as determined by permutational multivariate analysis of variance (PERMANOVA) (Figure 5B). To assess the similarity between FMT recipient mice and their respective donors or PBS recipient controls, we thus calculated unweighted UniFrac distances demonstrating a unique hybrid microbiome of FMT mice that significantly differed from both the donors and PBS recipient controls for either 2DC FMT or control FMT (Figure 5C). Importantly, *Lactobacillus*, as a top taxon enriched in 2DG-treated donors, was also significantly increased in 2DG-FMT mice, which also demonstrated elevated abundance of *Parabacteroides* and *Coprobacillus* (order Erysipelotrichales) (Figures 1F and 5D). In contrast, levels of AF12 were found to be higher in both the Ctrl donors and Ctrl-FMT mice, when compared to their 2DG counterparts (Figures 1F and 5D). In addition, *Bilophila* (family Desulfovibrionaceae) was also enriched in Ctrl-FMT mice. Bacteroidales that were absent
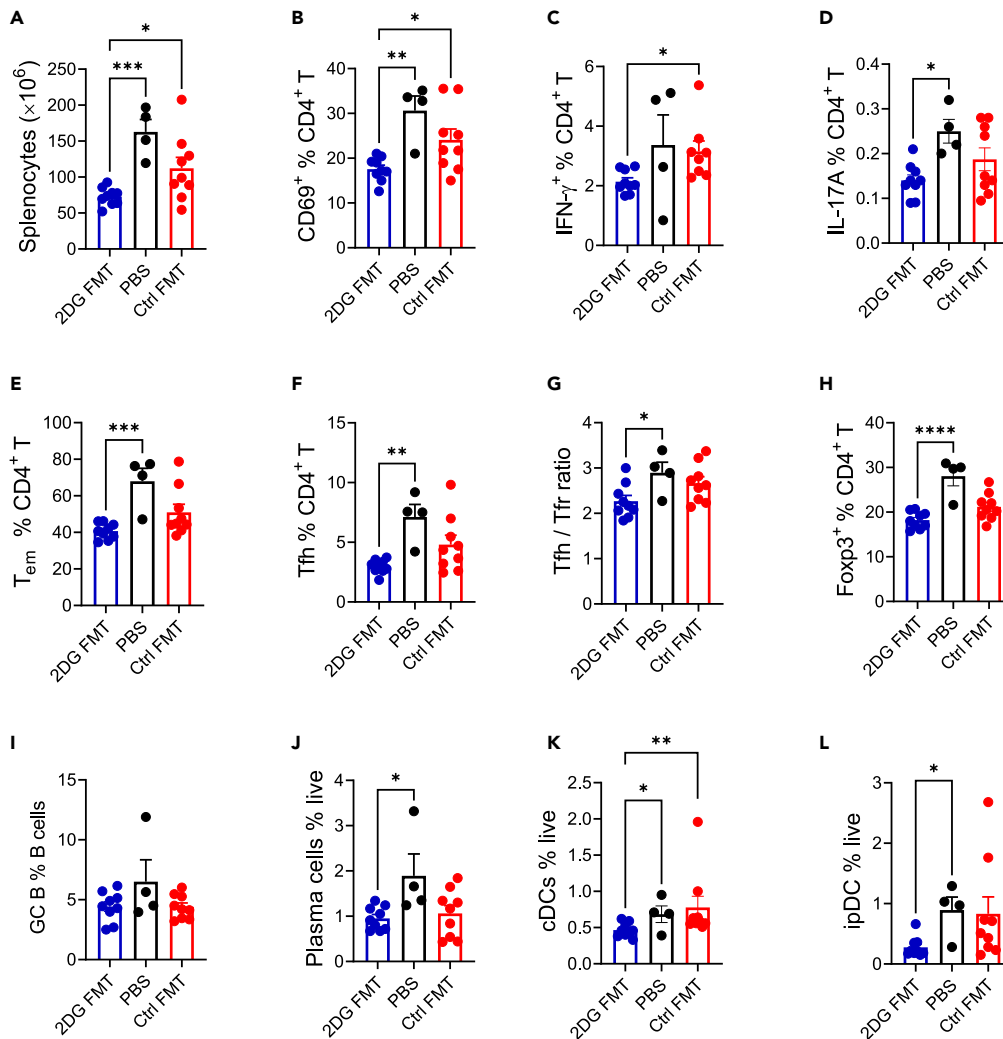
Figure 4. FMT from 2DG-treated mice reduced immune activation in BWF1 mice

Splenic cells from 2DG-FMT, Ctrl-FMT and PBS mice were analyzed after 20 weeks of FMT.

(A) Splenocyte numbers.

(B–L) Frequency of CD4$^+$ T cells expressing CD69, IFNγ (C) or IL–17A (D) and presenting the CD62L$^-$CD44$^+$ Tem phenotype (E). Frequency of Tfh cells (F) with the ratio of Tfh to Tfr cells (G). Frequency of Foxp3$^+$CD4$^+$T cells (H), GC B cells (I), CD138$^+$B220^{lo} plasma cells (J), CD11c$^+$MHC-II$^+$ cDCs (K), and CD11b$^-$pDCA$^+$B220$^-$ ipDCs (L). Each symbol represents a mouse, bars show means ± SEM. n = 4–10 per group. One-way ANOVA with Dunnett's (A, B, D-J) or Kruskal-Wallis (C, K and L) multiple comparison tests, *p < 0.05, **p < 0.01, ***p < 0.001 and ****p < 0.0001. See also Figure S3.

in 2DG donors (zero in 2DG versus 1.06% on average in Ctrl donors) (Figure 1F), gained colonization in 2DG-FMT mice (Figure 5D). Together, these results suggest that 2DG-dependent microbiome signature is largely transferable through FMT.

2DG treatment ameliorated disease in the (NZW x BXSB)F1 mouse model of lupus

To investigate whether the protective effect of FMT from 2DG-treated mice may be model-dependent, we used male (NZW x BXSB)F1 mice (WYaa), which develop an aggressive lupus-like syndrome driven by the duplication of the *Tlr7* gene to the Y chromosome.[29] First, we verified the effect of 2DG on disease progression in these mice. We studied the effect of a 4-week treatment starting at age 10–12 weeks, when WYaa mice start producing autoantibodies. Consistent with observations in BWF1 mice (Figure S1), 2DG reduced splenomegaly (Figure S4A), kidney pathology (Figures S4B and S4C), as well as C3 and IgG2a immune complex deposition, and renal infiltration of T cells and F4/80$^+$ macrophages (Figures S4D and S4E).
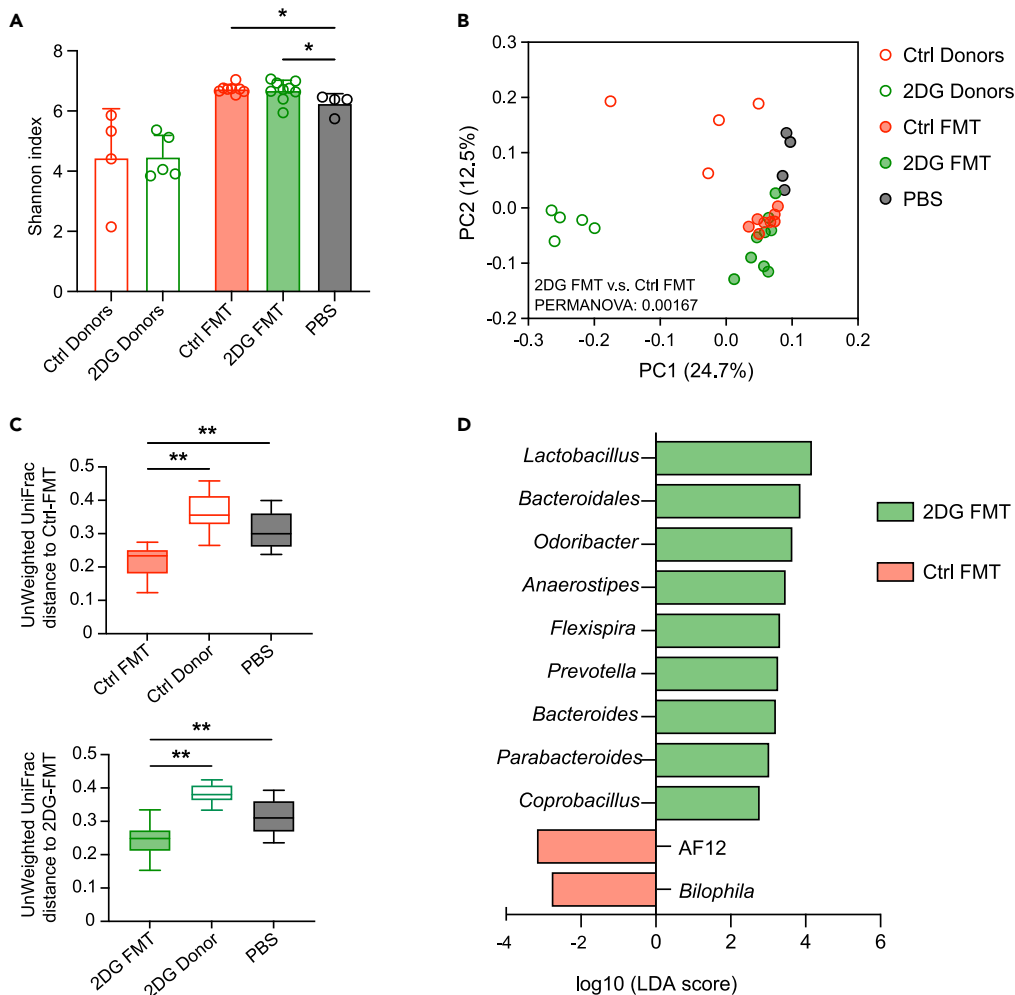
Figure 5. FMT from 2DG-treated mice results in a hybrid microbial signature in BWF1 mice

(A) Shannon index measuring bacterial alpha-diversity in 2DG-FMT (n = 9 per group), Ctrl-FMT (n = 8 per group), and PBS controls (n = 4 per group). The 2DG and Ctrl donors (n = 4–5 per group) at age 46 weeks were also included. Significance: *p < 0.05, One-way ANOVA with Dunnett's multiple comparison tests.

(B) Unweighted Unifrac PCoA plot showing the bacterial community structure.

(C) Unweighted UniFrac distances depicting the dissimilarity between the FMT mice and their respective donors or PBS recipients. Significance: **q < 0.001, PERMANOVA.

(D) LEfSe plot showing differentiating taxa (species level) between 2DG-FMT and Ctrl-FMT mice.

Furthermore, 2DG lowered the production of serum ANA and anti-dsDNA IgG (Figures S4F and S4G), as well as the frequency of activated $CD4^+$ $CD69^+$ T cells, Tem, Tfh cells, GC B, and PC cells compared to control mice (Figures S4H–S4L).

The 2DG treatment impacted the composition and the associated metabolites of the fecal microbiota in WYaa mice

16S rRNA sequencing of fecal samples collected from WYaa mice before and after 2DG treatment demonstrated a significant increase in alpha-diversity by 2DG, as measured by Shannon index (Figure 6A). At bacterial phylum level, there was a trend toward decreased *Bacteroidetes* and increased *Firmicutes* after 2DG treatment (Figure 6B). As observed in BWF1 mice, 2DG also increased the relative abundance of *Lactobacillus* and *Erysipelotrichaceae* in WYaa mice (Figures 6C and S5A). *Coprococcus*, and *Anaerofustis* of the class Clostridia producing butyrate were also enriched in 2DG-administrated mice, wherein the opportunistic pathogen *Staphylococcus* was reduced (Figure 6C). Consistent with these differences in distribution,
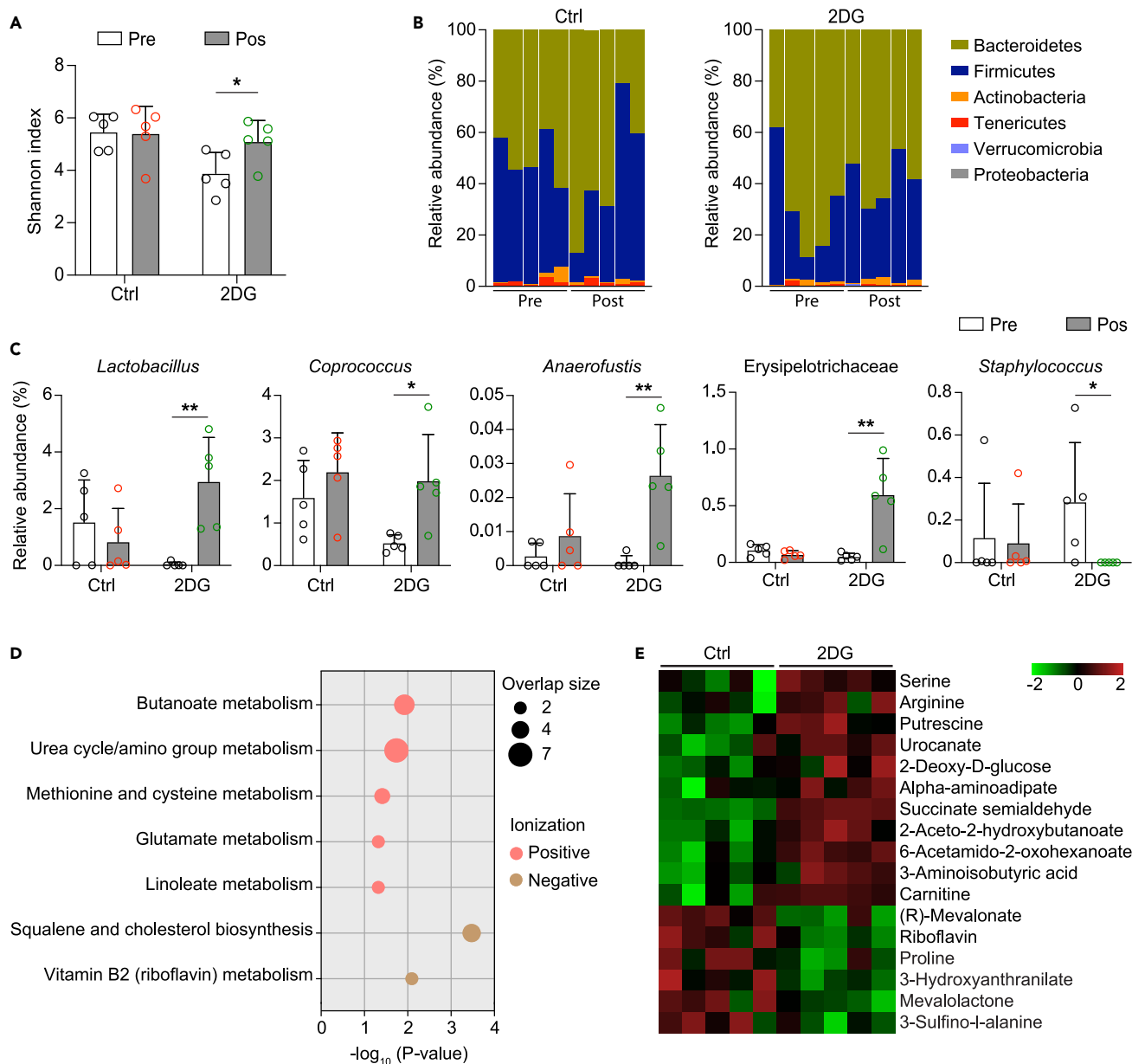
Figure 6. 2DG modulated fecal microbiota composition and metabolites in WYaa mice

Fecal samples were collected from WYaa mice pre- and post 2DG treatment to analyze microbiota composition and associated metabolites (n = 5 per group).

(A) Shannon index measuring bacterial diversity.

(B) Relative abundance of bacterial phyla pre- and post-treatment in the control and treated groups.

(C) Major differential taxa induced by 2DG treatment. Metabolic pathways (D) and metabolites (E) differentially enriched in the fecal samples collected from 2DG-treated WYaa mice versus untreated controls. Bar indicates mean and SD. *p < 0.05; **p < 0.01; two-tailed unpaired t test (A) and Mann–Whitney U test (C). See also Figures S4 and S5.

butyrate (butanoate) metabolism was a major metabolic pathway enriched by the 2DG treatment (Figure 6D), as shown by enriched metabolites in this pathway, including succinate semialdehyde, 2-aceto-2-hydroxybutanoate, and 3-aminoisobutyric acid (Figure 6E). In addition, serine, arginine, putrescine, and carnitine were found at higher levels not only in BWF1 but also in WYaa mice treated with 2DG (Figures 6E and S5B). A tryptophan metabolite, 3-hydroxyanthranilate, was reduced in WYaa mice treated with 2DG (Figure 6E). These results, thus, indicate that the regulation of gut microbiota and associated

metabolic activities by 2DG is mouse-model independent. Bacteria taxa and metabolites shared between the two strains in response to 2DG may point to candidates that are responsible for the protective effect of 2DG FMT.

FMT from 2DG-treated mice ameliorated disease in WYaa mice

To demonstrate whether the changes induced by 2DG in the WYaa microbiota may exert functional consequences, we followed a similar FMT protocol used for the BWF1 mice. Here, 3-week-old WYaa mice were treated with an antibiotic cocktail for 2 weeks, and then gavaged with feces from 2DG or untreated donor mice 3 times a week for 9 weeks (Figure S2B). A group of mice, serving as controls, were gavaged with PBS. As with BWF1 mice, 2DG-FMT reduced kidney pathology as compared to the Ctrl-FMT treatment in WYaa mice (Figures 7A and 7B). The glomeruli of all PBS-treated and Ctrl-FMT mice exhibited severe mesangial, and endocapillary hyperplasia with "wire-loop" lesions. In addition, glomeruli from all Ctrl-FMT mice presented extensive mesangial hyaline deposits. PBS-treated and Ctrl-FMT mice also showed acute tubular injury with dilatation, epithelial attenuation, accumulation of protein resorption droplets, and casts. One 2DG-FMT mouse demonstrated an early disease that developed faster than in PBS-treated group and Ctrl-FMT mice, and it had to be euthanized early. The other 2DG-FMT mice showed a normal renal cortex with very few hypercellular glomeruli. One mouse exhibited heavy mesangial hyaline deposits, but with patent, i.e. non-damaged, capillary loops. Although there were only small effects on C3 and IgG2a immune complex deposition, infiltration of $CD3^+$ T cells and $F4/80^+$ macrophages were also diminished in 2DG-FMT compared to Ctrl-FMT mice (Figures 7C and 7D). Production of ANA was reduced with 2DG-FMT treatment (Figure 7E), with a similar trend for anti-dsDNA IgG (Figure 7F).

Next, we examined the effect of 2DG-FMT on immune phenotypes. 2DG-FMT reduced splenomegaly (Figure 8A) as well as the frequencies of activated $CD4^+ CD69^+$ T cells, and Tem cells as compared to Ctrl-FMT (Figures 8B and 8C). Although it demonstrated no effect on the frequency of $IFN\gamma^+ CD4^+T$ cells (Figure 8D), 2DG-FMT reduced the frequency of $IL-17A^+ CD4^+$ T cells compared to Ctrl-FMT (Figure 8E). Moreover, the frequency of Tfh cells was reduced by 2DG-FMT compared to both control groups, and the ratio of Tfh to Tfr cells as well as the frequency of $Foxp3^+$ regulatory $CD4^+$ T cells were reduced in 2DG-FMT compared to the PBS group (Figures 8F–8H). The frequency of GC B cells or plasma cells was unaffected (Figures 8I and 8J); however, the frequencies of class-switched B cells, which depends on Tfh cells, and age-related B cells (ABCs), a subset of pathogenic type I IFN-driven B cells, were reduced by 2DG-FMT compared to Ctrl-FMT (Figures 8K and 8L). Similar results were obtained from the mLN where 2DG-FMT mice showed smaller mLNs with lower cell numbers compared to Ctrl-FMT mice (Figure S6A). 2DG-FMT reduced the frequency of mLN Tem cells and Tfh cells as well as $IFN\gamma^+$, and $IL-17A^+ CD4^+$ T cells compared to Ctrl-FMT mice (Figures S6B–S6E). Once again, the frequency of GC B cells was unaffected (Figure S6F), however, the frequency of plasma cells, CS B cells, and ABCs was significantly reduced by 2DG-FMT (Figures S6G–S6I).

Finally, increased TLR7 signaling drives a myeloid expansion in Yaa-carrying mice.[22] The 2DG-FMT treatment reduced the frequency of splenic $CD11b^+$ cells as compared to both control groups (Figure 9A). The frequency of $Ly6C^+CD11b^+$ monocytes, $F4/80^+CD11b^+$ macrophages, cDCs, and ipDCs was reduced in 2DG-FMT compared to Ctrl-FMT mice (Figures 9B–9E). A similar effect was observed in mLN myeloid cells (Figure S7). Together, these results indicate that the protective effect of FMT from 2DG-treated lupus-prone mice is model-independent. However, contrary to BWF1 mice in which FMT from control mice showed intermediate results between 2DG-FMT and PBS, FMT from control mice seemed to accelerate disease in WYaa mice. Overall, 2DG-FMT was protective, although in this latter model wherein the disease develops very rapidly, it was not protective in all mice compared to BWF1 mice in which the disease evolves at a slower pace.

DISCUSSION

Results obtained in mouse models suggest that the gut microbial dysbiosis observed in SLE patients contributes to the disease process.[30,31] There is also emerging evidence that the microbiota composition may globally modulate the host response to therapies,[32] including in autoimmune diseases such as rheumatoid arthritis, in which the gut microbiome can predict the response of patients to methotrexate.[33] Here, we tested the hypothesis that the gut microbiome plays a role in the therapeutic response of lupus-prone mice to the inhibition of glycolysis, a metabolic pathway that is overactivated in lupus $CD4^+$ T cells[15] and B cells.[34] This hypothesis was based on a model in which the metabolic inhibitor metformin exerts
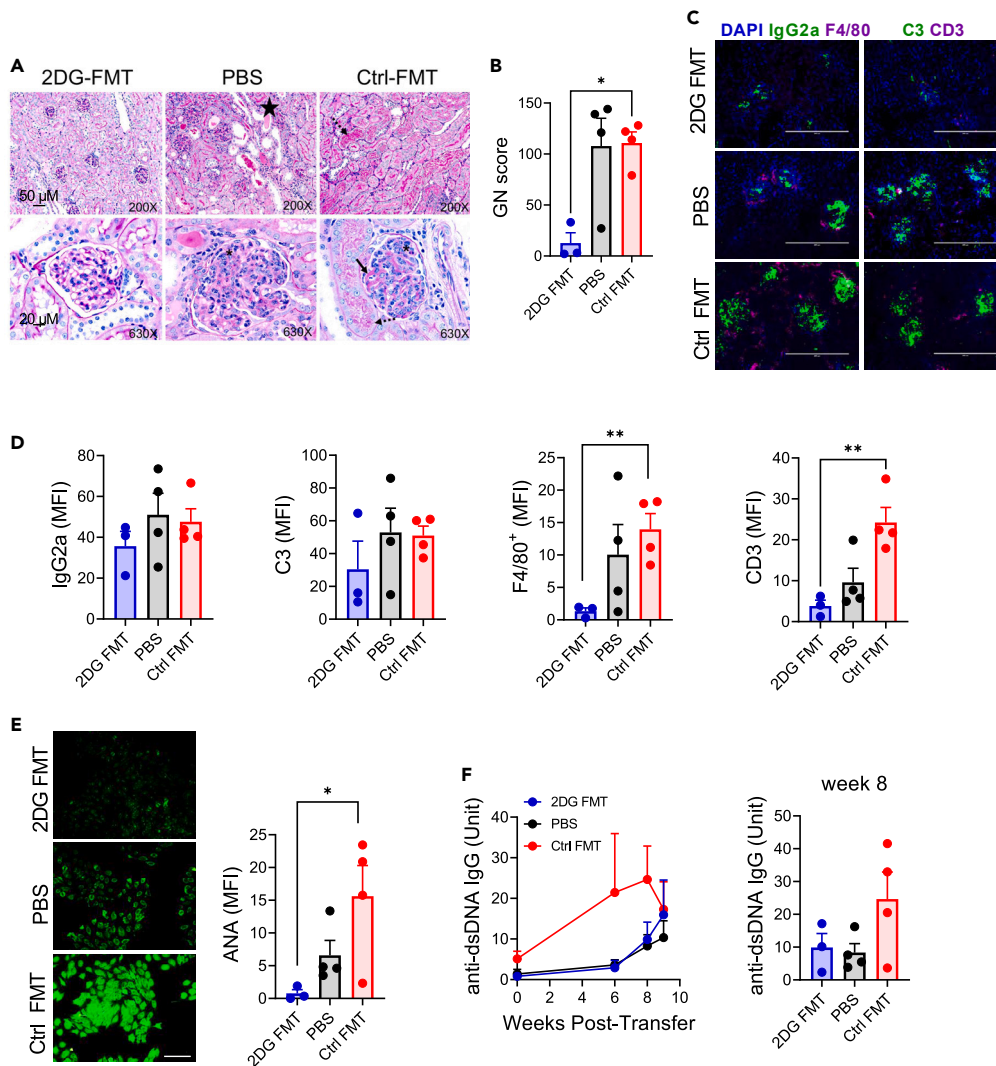
Figure 7. FMT from 2DG treated mice reduced renal pathology and autoantibody production in WYaa mice

Antibiotic-pretreated 5-week-old WYaa mice received 2DG-FMT, Ctrl-FMT or PBS for 9 weeks.

(A) Representative PAS-stained kidney sections at 200X (top, scale bar 50 μM) and 630X (bottom, scale bar 20 μM) magnifications. The * symbols indicate endocapillary hypercellularity, the star symbol shows a cast, dashed arrows show protein droplets in dilated proximal tubules and plain arrows show "wire-loop" peripheral hyaline deposits.

(B and C) GN scores (C) Representative images of IgG2a and F4/80+ macrophages, and C3 and CD3+ T cells in glomeruli (20x, scale bars: 100 μM).

(D) Quantification of IgG2a, C3, F4/80 and CD3 (MFI).

(E) Representative images of terminal serum ANA (20x) and ANA intensity quantification (MFI).

(F) Time course of serum anti-dsDNA IgG and values at week 8. Each symbol represents a mouse, bars show means ± SEM. N = 3–4 mice per group. One-way ANOVA with Dunnett's or Kruskal-Wallis (B) multiple comparison tests, *p < 0.05, **p < 0.01, and ***p < 0.001. See also Figure S2.

its therapeutic effects in type 2 diabetes at least in part by altering the composition of the gut microbiome.[20,21]

We selected the BWF1 and WYaa models of lupus that have different etiologies and in which microbial dysbiosis has been documented.[3,7] We showed here that, as for other models of lupus, including BWF1,[15,16] 2DG has a therapeutic effect in WYaa mice. We then demonstrated that the composition of the gut microbiota and the metabolites it produces were changed by 2DG in both models. The 2DG treatment reduced the changes in microbiota composition associated with disease progression in untreated BWF1 mice, and it
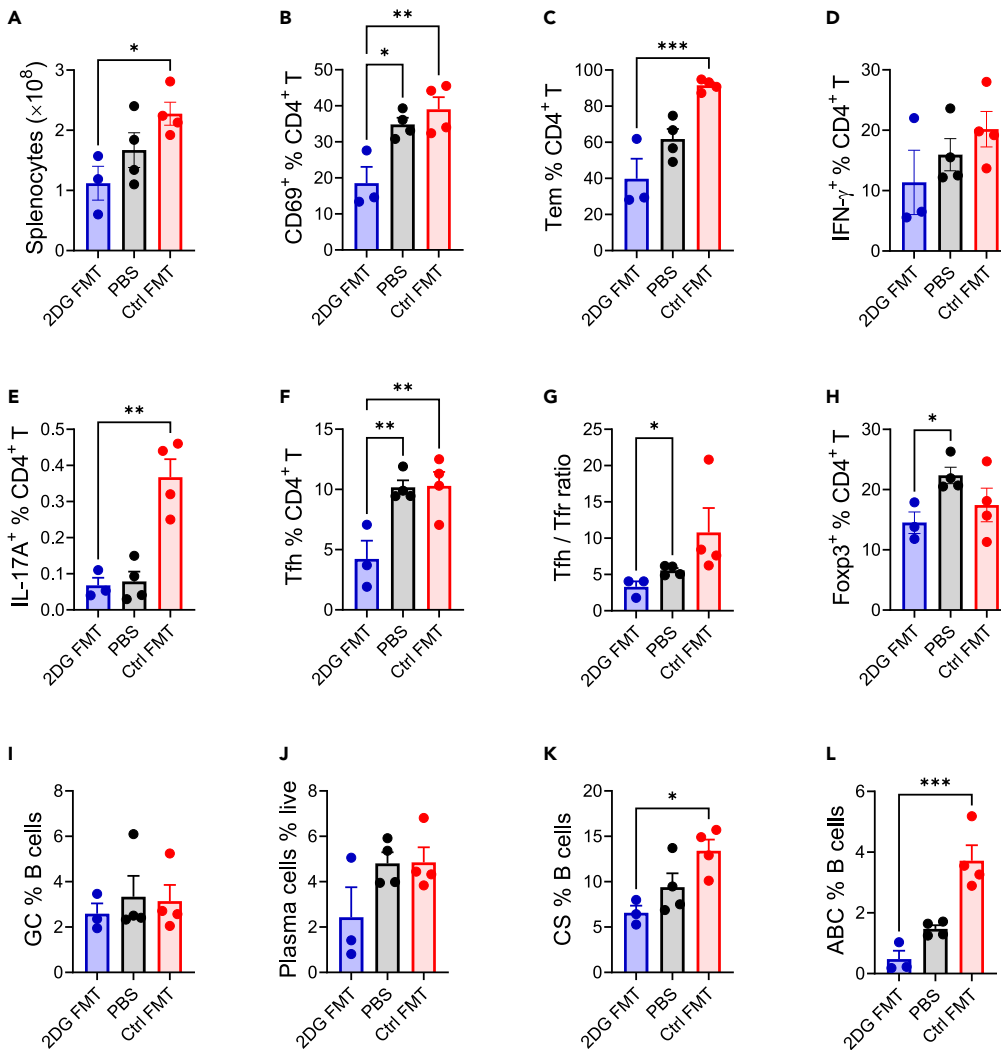
Figure 8. 2DG-FMT treatment reduced lymphocyte activation in WYaa mice

Splenic cells were analyzed after 9 weeks of FMT.

(A) Splenocyte numbers.

(B–L) Frequency of $CD4^+$ T cells expressing CD69, presenting a Tem phenotype (C), expressing IFNγ (D) or IL-17A (E). Frequency of Tfh cells (F) with the ratio of Tfh to Tfr cells (G). Frequency of $Foxp3^+CD4^+$T cells (H), GC B cells (I), PCs (J), $CD19^+IgM^-IgD^-$class-switched (CS) B cells (K) and $TBET^+CD11c^+$ B cells (ABCs) (L). Each symbol represents a mouse, bars show means ± SEM. N = 3–4 per group. One-way ANOVA with Dunnett's multiple comparison tests, *p < 0.05, **p < 0.01, ***p < 0.001 and ****p < 0.0001. See also Figure S6.

increased alpha diversity and the *Firmicutes* to *Bacteroides* ratio in WYaa mice. A common effect of 2DG was observed in the two strains, with a decreased abundance of bacterial taxonomic groups associated with lupus and inflammation. In both strains, the distribution of fecal metabolites was also altered by the treatment in both strains, most likely reflecting changes in the distribution of bacterial species. This included changes in tryptophan metabolites, and alterations in tryptophan catabolism by the gut micro-biome have been functionally validated in a mouse model of lupus.[11,27] Here, we found that 2DG increased the abundance of fecal tryptophan and kynurenine in BWF1 mice, and the amount of 3-hydroxyanthranilate, a kynurenine metabolite that may be of either mammalian or bacterial origins, was decreased in WYaa mice. Of interest, a high level of 3-hydroxyanthranilate was found in B6.*Sle1.Sle2.-Sle3* mice as compared to control B6 mice, and it was reduced by low dietary tryptophan, which decreased autoimmune activation.[27] This may indicate that 2DG may exert a beneficial effect in part by decreasing tryptophan bacterial catabolism, although the mechanism by which this may occur is unclear. However,
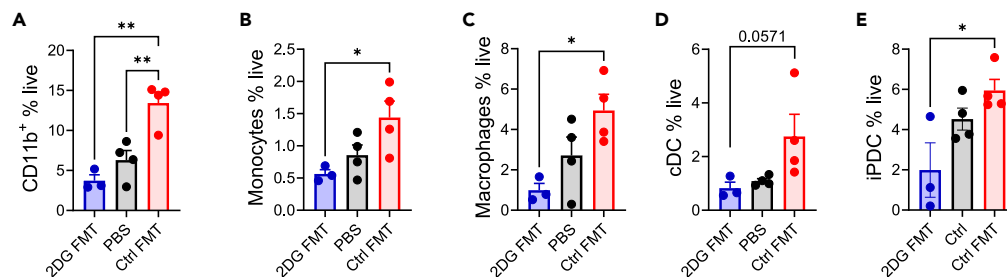
Figure 9. 2DG-FMT treatment reduced myeloid cell expansion in WYaa mice

(A–E) Splenic myeloid cells were analyzed after 9 weeks of FMT transfer. Frequency of CD11b$^+$ cells (A), Ly6C$^+$ monocytes (B) and F4/80$^+$ macrophages (C). Frequency of cDCs (D) and ipDCs (E). Each symbol represents a mouse, bars show means ± SEM. N = 3–4 per group. One-way ANOVA with Dunnett's multiple comparison tests, *p < 0.05, **p < 0.01. See also Figure S7.

the mechanism(s) by which specific metabolites may modulate the host immunity should be interpreted with caution. The increased production of butyrate derivatives observed in fecal samples of 2DG-treated WYaa mice did not correspond to an expected expansion of Treg cells in either 2DG-treated mice themselves,[15] or in the recipients of these fecal contents (this report). It is thus possible that SCFA modulate other components of the immune system directly, or indirectly through intestinal stromal cells.

To test whether the changes in microbiota induced by 2DG had functional consequences, we assessed whether FMT transfer from 2DG-treated mice could prevent disease in young mice of the same strain. In BWF1 mice, 2DG-FMT decreased the production of autoantibodies and prevented the development of glomerulonephritis, including immune complex deposition and immune cell infiltration. Similar results were observed in WYaa mice, although the effect was more modest, which could be because of a faster disease development in this model, or to a lower protection of the 2DG-altered microbiota relative to the strong TLR7-driven inflammation. In both strains, the 2DG-FMT reduced the activation of CD4$^+$ T cells, and their differentiation in Tem and Tfh subsets, as well as the activation of myeloid cells. The protective effect on B cells was limited to class-switching, which can be imparted to the reduced numbers of Tfh cells, and in plasma cells, which could also be indirect targets. FMT transfer from control mice resulted in intermediate autoantibody production and expression of some activation markers between 2DG-FMT and PBS control mice in the BWF1 strain. In WYaa mice however, recipients of FMT from control mice showed worsening of disease development compared to PBS as compared to PBS treated mice. The mechanism responsible for this difference is unclear, and could be of either bacterial or host origins, or both. Transfers across these two strains will be necessary to start addressing this issue.

We showed that 2DG functionally changed the gut microbiota of lupus-prone mice, but whether it was a direct effect on bacterial populations or an indirect effect through the modification of the immune system that in turn altered the microbiota is unknown. A treatment was developed with a combination of metformin and 2DG that ameliorated gastric cancer induced by *Heliobacter pilori* in a murine model.[35] This was accomplished without affecting the bacterial burden, but by decreasing host cells glycolysis and mTOR activation in infected cells. *Citrobacter rodentium*-induced intestinal injury was equally reduced by a treatment with 2DG or antibiotics, implying that 2DG mitigated the microbiome with beneficial effects,[36] although it was not directly demonstrated as we did with lupus-prone mice. A causal effect of the host cellular metabolism on the gut microbiome has been shown where mitochondrial (mt) ROS production linked to a mtDNA polymorphism in the NZB mouse, one of the parental strains in the BWF1 model, altered the gut microbiome, including a reduction of bacterial diversity and of the *Firmicutes/Bacteroides* ratio.[37] Treatment of these NZB mice with N-acetylcysteine (NAC), a ROS scavenger with a therapeutic effect in SLE patients,[38] reversed the changes in the microbiome. However, NZB mice develop minimal autoimmune pathogenesis, and this study did not address the link between the normalization of the gut microbiome by NAC and autoimmune phenotypes. Direct causal links between changes induced by a drug or an environmental modification on the microbiome and phenotypic/disease changes in the host requires either FMT, as we did in this study, or bacterial colonization.

Finally, dietary sugar has been shown to alter the gut microbiome by promoting the expansion of a pathobiont that outcompeted segmented filamentous commensal bacteria (SFB).[39] SFB promoted the

differentiation of intestinal Th17 and ILC3 cells, which were essential to maintain gut homeostasis as well as to limit the absorption of dietary lipids. Therefore, in this model, sugar directly modified the microbiome, which in turn shaped the immune system with systemic outcomes. Although it has not been formally tested, it is likely that 2DG inhibits bacterial glycolysis, since the obligate phosphorylation of glucose is conserved across organisms. It is thus possible that 2DG acts directly on bacteria by promoting the growth of taxa that are less dependent on glucose metabolism.

Thus, we have shown that the protective effect of 2DG in lupus-prone mice and the pathogenic effect of the dysbiotic gut microbiota on autoimmune pathogenesis in these mice are linked. 2DG changed the microbiota, which can largely transfer the protective effect of the treatment itself. These results are similar to those obtained with metformin in type 2 diabetes. This suggests that the microbiome should be considered as an integral part of the immunometabolic activation that has been documented in immune mediated diseases, and in their treatment with metabolic inhibitors.

Limitations of the study

This study demonstrated that the enhanced glucose metabolism that is required for lupus pathogenesis is functionally linked to gut microbial dysbiosis. There are two main limitations to the study. First, although we have shown that the inhibition of glucose metabolism greatly modified the composition of the gut microbiota of lupus-prone mice and the metabolites it produced, we have not yet identified the bacteria or metabolites that are responsible for the protective effect it has on lupus development. The second limitation is that although both enhanced glucose metabolism and gut dysbiosis have been documented in SLE patients, it is unknown yet if the functional link that we report in mice exists in humans.

STAR★METHODS

Detailed methods are provided in the online version of this paper and include the following:

- KEY RESOURCES TABLE
- RESOURCE AVAILABILITY
  - Lead contact
  - Materials availability
  - Data and code availability
- EXPERIMENTAL MODEL AND STUDY PARTICIPANT DETAILS
- METHOD DETAILS
  - Study design
  - Mouse treatments
  - Renal pathology
  - Autoantibody measurement
  - Gut microbiota sequence analysis
  - Fecal metabolomic analysis
  - Flow cytometry
- QUANTIFICATION AND STATISTICAL ANALYSIS

SUPPLEMENTAL INFORMATION

Supplemental information can be found online at https://doi.org/10.1016/j.isci.2023.107122.

AUTHOR CONTRIBUTIONS

A.S.E., J.B., N.K., M.Z., G.A., and S.C.C. performed the experimental studies. Y.G. performed the computational studies. T.J.G. supervised the metabolomic analysis, W.C. scored the renal pathology. G.S. and L.M. designed the study. M.M. and L.M. supervised the work and wrote the manuscript. All authors assisted in manuscript preparation.

DECLARATION OF INTERESTS

The authors declare no competing interests.

INCLUSION AND DIVERSITY

We support inclusive, diverse and equitable conduct of research.

REFERENCES

1. Tsokos, G.C. (2011). Systemic lupus erythematosus. N. Engl. J. Med. *365*, 2110–2121.

2. Hevia, A., Milani, C., López, P., Cuervo, A., Arboleya, S., Duranti, S., Turroni, F., González, S., Suárez, A., Gueimonde, M., et al. (2014). Intestinal dysbiosis associated with systemic lupus erythematosus. mBio *5*, e01548-14. https://doi.org/10.1128/mBio.01548-14.

3. Luo, X.M., Edwards, M.R., Mu, Q., Yu, Y., Vieson, M.D., Reilly, C.M., Ahmed, S.A., and Bankole, A.A. (2018). Gut Microbiota in Human Systemic Lupus Erythematosus and a Mouse Model of Lupus. Appl. Environ. Microbiol. *84*, e02288-17. https://doi.org/10.1128/AEM.02288-17.

4. He, Z., Shao, T., Li, H., Xie, Z., and Wen, C. (2016). Alterations of the gut microbiome in Chinese patients with systemic lupus erythematosus. Gut Pathog. *8*, 64. https://doi.org/10.1186/s13099-016-0146-9.

5. Azzouz, D., Omarbekova, A., Heguy, A., Schwudke, D., Gisch, N., Rovin, B.H., Caricchio, R., Buyon, J.P., Alekseyenko, A.V., and Silverman, G.J. (2019). Lupus nephritis is linked to disease-activity associated expansions and immunity to a gut commensal. Ann. Rheum. Dis. *78*, 947–956. https://doi.org/10.1136/annrheumdis-2018-214856.

6. Christovich, A., and Luo, X.M. (2022). Gut Microbiota, Leaky Gut, and Autoimmune Diseases. Front. Immunol. *13*, 946248. https://doi.org/10.3389/fimmu.2022.946248.

7. Manfredo Vieira, S., Hiltensperger, M., Kumar, V., Zegarra-Ruiz, D., Dehner, C., Khan, N., Costa, F.R.C., Tiniakou, E., Greiling, T., Ruff, W., et al. (2018). Translocation of a gut pathobiont drives autoimmunity in mice and humans. Science *359*, 1156–1161. https://doi.org/10.1126/science.aar7201.

8. Bagavant, H., Araszkiewicz, A.M., Ingram, J.K., Cizio, K., Merrill, J.T., Arriens, C., Guthridge, J.M., James, J.A., and Deshmukh, U.S. (2021). Immune response to Enterococcus gallinarum in lupus Patients is associated with a subset of lupus-associated autoantibodies. Front. Immunol. *12*, 635072. https://doi.org/10.3389/fimmu.2021.635072.

9. Zegarra-Ruiz, D.F., El Beidaq, A., Iñiguez, A.J., Lubrano Di Ricco, M., Manfredo Vieira, S., Ruff, W.E., Mubiru, D., Fine, R.L., Sterpka, J., Greiling, T.M., et al. (2019). A diet-sensitive commensal Lactobacillus strain mediates TLR7-dependent systemic autoimmunity. Cell Host Microbe *25*, 113–127.e6. https://doi.org/10.1016/j.chom.2018.11.009.

10. Silverman, G.J., Deng, J., and Azzouz, D.F. (2022). Sex-dependent Lupus Blautia (Ruminococcus) gnavus strain induction of zonulin-mediated intestinal permeability and autoimmunity. Front. Immunol. *13*, 897971. https://doi.org/10.3389/fimmu.2022.897971.

11. Choi, S.C., Brown, J., Gong, M., Ge, Y., Zadeh, M., Li, W., Croker, B.P., Michailidis, G., Garrett, T.J., Mohamadzadeh, M., and Morel, L. (2020). Gut microbiota dysbiosis and altered tryptophan catabolism contribute to autoimmunity in lupus-susceptible mice. Sci. Transl. Med. *12*, eaax2220. https://doi.org/10.1126/scitranslmed.aax2220.

12. Ma, Y., Xu, X., Li, M., Cai, J., Wei, Q., and Niu, H. (2019). Gut microbiota promote the inflammatory response in the pathogenesis of systemic lupus erythematosus. Mol. Med. *25*, 35. https://doi.org/10.1186/s10020-019-0102-5.

13. Sharabi, A., and Tsokos, G.C. (2020). T cell metabolism: new insights in systemic lupus erythematosus pathogenesis and therapy. Nat. Rev. Rheumatol. *16*, 100–112. https://doi.org/10.1038/s41584-019-0356-x.

14. Teng, X., Cornaby, C., Li, W., and Morel, L. (2019). Metabolic regulation of pathogenic autoimmunity: therapeutic targeting. Curr. Opin. Immunol. *61*, 10–16. https://doi.org/10.1016/j.coi.2019.07.001.

15. Yin, Y., Choi, S.C., Xu, Z., Perry, D.J., Seay, H., Croker, B.P., Sobel, E.S., Brusko, T.M., and Morel, L. (2015). Normalization of CD4+ T cell metabolism reverses lupus. Sci. Transl. Med. *7*, 274ra18. https://doi.org/10.1126/scitranslmed.aaa0835.

16. Choi, S.C., Titov, A.A., Abboud, G., Seay, H.R., Brusko, T.M., Roopenian, D.C., Salek-Ardakani, S., and Morel, L. (2018). Inhibition of glucose metabolism selectively targets autoreactive follicular helper T cells. Nat. Commun. *9*, 4369. https://doi.org/10.1038/s41467-018-06686-0.

17. Yin, Y., Choi, S.-C., Xu, Z., Zeumer, L., Kanda, N., Croker, B.P., and Morel, L. (2016). Glucose oxidation is critical for CD4+ T cell activation in a mouse model of systemic lupus erythematosus. J. Immunol. *196*, 80–90. https://doi.org/10.4049/jimmunol.1501537.

18. Titov, A.A., Baker, H.V., Brusko, T.M., Sobel, E.S., and Morel, L. (2019). Metformin inhibits the type 1 IFN response in human CD4(+) T cells. J. Immunol. *203*, 338–348. https://doi.org/10.4049/jimmunol.1801651.

19. Sun, F., Wang, H.J., Liu, Z., Geng, S., Wang, H.T., Wang, X., Li, T., Morel, L., Wan, W., Lu, L., et al. (2020). Safety and efficacy of metformin in systemic lupus erythematosus: a multicentre, randomised, double-blind, placebo-controlled trial. The Lancet Rheumatology *2*, e210–e216. https://doi.org/10.1016/s2665-9913(20)30004-7.

20. Shin, N.-R., Lee, J.-C., Lee, H.-Y., Kim, M.-S., Whon, T.W., Lee, M.-S., and Bae, J.-W. (2014). An increase in the Akkermansia spp. population induced by metformin treatment improves glucose homeostasis in diet-induced obese mice. Gut *63*, 727–735. https://doi.org/10.1136/gutjnl-2012-303839.

21. Forslund, K., Hildebrand, F., Nielsen, T., Falony, G., Le Chatelier, E., Sunagawa, S., Prifti, E., Vieira-Silva, S., Gudmundsdottir, V., Pedersen, H.K., et al. (2015). Disentangling type 2 diabetes and metformin treatment signatures in the human gut microbiota. Nature *528*, 262–266. https://doi.org/10.1038/nature15766.

22. Hang, L.M., Izui, S., and Dixon, F.J. (1981). (NZW x BXSB)F1 hybrid. A model of acute lupus and coronary vascular disease with myocardial infarction. J. Exp. Med. *154*, 216–221. https://doi.org/10.1084/jem.154.1.216.

23. Toumi, E., Goutorbe, B., Plauzolles, A., Bonnet, M., Mezouar, S., Militello, M., Mege, J.L., Chiche, L., and Halfon, P. (2022). Gut microbiota in systemic lupus erythematosus patients and lupus mouse model: a cross species comparative analysis for biomarker discovery. Front. Immunol. *13*, 943241. https://doi.org/10.3389/fimmu.2022.943241.

24. de la Visitacion, N., Robles-Vera, I., Toral, M., and Duarte, J. (2019). Protective Effects of Probiotic Consumption in Cardiovascular Disease in. Systemic Lupus Erythematosus. Nutrients *11*. https://doi.org/10.3390/nu11112676.

25. Pan, Q., Guo, F., Huang, Y., Li, A., Chen, S., Chen, J., Liu, H.F., and Pan, Q. (2021). Gut Microbiota Dysbiosis in Systemic Lupus Erythematosus: Novel Insights into Mechanisms and Promising Therapeutic Strategies. Front. Immunol. *12*, 799788. https://doi.org/10.3389/fimmu.2021.799788.

26. Kverka, M., Zakostelska, Z., Klimesova, K., Sokol, D., Hudcovic, T., Hrncir, T., Rossmann, P., Mrazek, J., Kopecny, J., Verdu, E.F., and Tlaskalova-Hogenova, H. (2011). Oral administration of Parabacteroides distasonis antigens attenuates experimental murine colitis through modulation of immunity and microbiota composition. Clin. Exp. Immunol. *163*, 250–259. https://doi.org/10.1111/j.1365-2249.2010.04286.x.

27. Brown, J., Abboud, G., Ma, L., Choi, S.-C., Kanda, N., Zeumer-Spataro, L., Lee, J., Peng, W., Cagmat, J., Faludi, T., et al. (2022). Microbiota-mediated skewing of tryptophan catabolism modulates CD4+ T cells in lupus-prone mice. iScience *25*, 104241. https://doi.org/10.1016/j.isci.2022.104241.

28. Zuniga, E.I., McGavern, D.B., Pruneda-Paz, J.L., Teng, C., and Oldstone, M.B.A. (2004). Bone marrow plasmacytoid dendritic cells can differentiate into myeloid dendritic cells upon virus infection. Nat. Immunol. *5*, 1227–1234. https://doi.org/10.1038/ni1136.

29. Hashimoto, Y., Kawamura, M., Ichikawa, K., Suzuki, T., Sumida, T., Yoshida, S., Matsuura, E., Ikehara, S., and Koike, T. (1992). Anticardiolipin antibodies in NZW x BXSB F1 mice. A model of antiphospholipid syndrome. J. Immunol. *149*, 1063–1068.

30. Silverman, G.J. (2019). The microbiome in SLE pathogenesis. Nat. Rev. Rheumatol. *15*, 72–74. https://doi.org/10.1038/s41584-018-0152-z.

31. Ruff, W.E., Greiling, T.M., and Kriegel, M.A. (2020). Host-microbiota interactions in immune-mediated diseases. Nat. Rev. Microbiol. *18*, 521–538. https://doi.org/10.1038/s41579-020-0367-2.

32. Hitch, T.C.A., Hall, L.J., Walsh, S.K., Leventhal, G.E., Slack, E., de Wouters, T., Walter, J., and Clavel, T. (2022). Microbiome-based interventions to modulate gut ecology and the immune system. Mucosal Immunol. *15*, 1095–1113. https://doi.org/10.1038/s41385-022-00564-1.

33. Nayak, R.R., Alexander, M., Deshpande, I., Stapleton-Gray, K., Rimal, B., Patterson, A.D., Ubeda, C., Scher, J.U., and Turnbaugh, P.J. (2021). Methotrexate impacts conserved pathways in diverse human gut bacteria leading to decreased host immune activation. Cell Host Microbe *29*, 362–377.e11. https://doi.org/10.1016/j.chom.2020.12.008.

34. Choi, S.C., Li, W., Zhang, X., Kanda, N., Zeumer-Spataro, L., Teng, X., and Morel, L. (2022). Pharmacologically inferred glycolysis and glutaminolysis requirement of B cells in lupus-prone mice. J. Immunol. *208*, 2098–2108. https://doi.org/10.4049/jimmunol.2100356.

35. Su, H., Bak, E.J., Kim, A., Tissera, K., Cha, J.H., and Jang, S. (2022). Helicobacter pylori-mediated gastric pathogenesis is attenuated by treatment of 2-deoxyglucose and metformin. J. Microbiol. *60*, 849–858. https://doi.org/10.1007/s12275-022-2130-z.

36. Ahmed, I., Verma, A., Umar, S., and Papineni, R.V.L. (2023). 2-deoxy-D-glucose mitigates Citrobacter rodentium and dibenzazepine-induced gastrointestinal damage and colitis: novel implications of 2-DG polypharmacopea. Int. J. Radiat. Biol. *99*, 681–691. https://doi.org/10.1080/09553002.2022.2110297.

37. Yardeni, T., Tanes, C.E., Bittinger, K., Mattei, L.M., Schaefer, P.M., Singh, L.N., Wu, G.D., Murdock, D.G., and Wallace, D.C. (2019). Host mitochondria influence gut microbiome diversity: A role for ROS. Sci. Signal. *12*, eaaw3159. https://doi.org/10.1126/scisignal.aaw3159.

38. Lai, Z.W., Hanczko, R., Bonilla, E., Caza, T.N., Clair, B., Bartos, A., Miklossy, G., Jimah, J., Doherty, E., Tily, H., et al. (2012). N-acetylcysteine reduces disease activity by blocking mammalian target of rapamycin in T cells from systemic lupus erythematosus patients: a randomized, double-blind, placebo-controlled trial. Arthritis Rheum. *64*, 2937–2946. https://doi.org/10.1002/art.34502.

39. Kawano, Y., Edwards, M., Huang, Y., Bilate, A.M., Araujo, L.P., Tanoue, T., Atarashi, K., Ladinsky, M.S., Reiner, S.L., Wang, H.H., et al. (2022). Microbiota imbalance induced by dietary sugar disrupts immune-mediated protection from metabolic syndrome. Cell *185*, 3501–3519.e20. https://doi.org/10.1016/j.cell.2022.08.005.

40. Elshikha, A.S., Teng, X.Y., Kanda, N., Li, W., Choi, S.C., Abboud, G., Terrell, M., Fredenburg, K., and Morel, L. (2022). TLR7 activation accelerates cardiovascular pathology in a mouse model of lupus. Front. Immunol. *13*, 914468. https://doi.org/10.3389/fimmu.2022.914468.

41. Morel, L., Mohan, C., Yu, Y., Croker, B.P., Tian, N., Deng, A., and Wakeland, E.K. (1997). Functional dissection of systemic lupus erythematosus using congenic mouse strains. J. Immunol. *158*, 6019–6028.

42. Ge, Y., Zadeh, M., and Mohamadzadeh, M. (2022). Vitamin B12 coordinates ileal epithelial cell and microbiota functions to resist Salmonella infection in mice. J. Exp. Med. *219*, e20220057. https://doi.org/10.1084/jem.20220057.

43. Kumar, A., Priyamvada, S., Ge, Y., Jayawardena, D., Singhal, M., Anbazhagan, A.N., Chatterjee, I., Dayal, A., Patel, M., Zadeh, K., et al. (2021). A Novel Role of SLC26A3 in the Maintenance of Intestinal Epithelial Barrier Integrity. Gastroenterology *160*, 1240–1255.e3. https://doi.org/10.1053/j.gastro.2020.11.008.

STAR★METHODS

KEY RESOURCES TABLE

REAGENT or RESOURCE	SOURCE	IDENTIFIER
Antibodies		
BCL-6 AF487	BD Biosciences	RRID:AB_10898007
CD3e APC	BD Biosciences	RRID:AB_398529
CD3e APC/Cy7	BD Biosciences	RRID:AB_396759
CD4 APC	BioLegend	RRID:AB_312718
CD4 FITC	BioLegend	RRID:AB_312712
CD4 eFluor 450	eBioscience	RRID:AB_10718983
CD4 PE	eBioscience	RRID:AB_465510
CD5 APC	BD Biosciences	RRID:AB_398457
CD11b PercP / Cy5.5	BD Biosciences	RRID:AB_394002
CD11c BV421	BioLegend	RRID:AB_10897814
CD11c APC	BioLegend	RRID:AB_313778
CD11c PE / Cy7	BD Biosciences	RRID:AB_647251
CD16/CD32	BD Biosciences	RRID:AB_394655
CD45R/B220 PE-CF594	BD Biosciences	RRID:AB_11151901
CD45R/B220 BV711	BD Biosciences	RRID:AB_2738470
CD19 BV711	BioLegend	RRID:AB_2565970
CD19 eFluor 450	eBioscience	RRID:AB_1272124
CD21/CD35 APC/Cy7	BioLegend	RRID:AB_1953274
CD23 FITC	BioLegend	RRID:AB_312830
CD25 AF700	eBioscience	RRID:AB_891422
CD44 PE	BioLegend	RRID:AB_312959
CD62L APC	BD Biosciences	RRID:AB_398533
CD69 PR/Cy7	BioLegend	RRID: AB_493564
CD93 PE	BD Biosciences	RRID:AB_397003
CD95 biotin	BD Biosciences	RRID:AB_395328
CD138 APC	Biolegend	RRID: AB_10960141
CD279 eFluor 450	eBioscience	RRID:AB_11150068
CD317 PE/Cy7	eBioscience	RRID:AB_2573440
Complement C3-FITC	ThermoFisher	RRID:AB_1954681
F4/80 APC	eBioscience	RRID:AB_2784648
F4/80 PE	eBioscience	RRID:AB_465923
FOXP3 FITC	eBioscience	RRID:AB_465243
FOXP3 PE	eBioscience	RRID:AB_465936
GL7 eFluor 450	eBioscience	RRID:AB_10870775
IFN-γ PB	BioLegend	RRID:AB_528922
IL-10 PE/Cy7	BioLegend	RRID:AB_11149682
IL-17A PE	Biolegend	RRID:AB_315463
Ly-6C AF700	Biolegend	RRID:AB_10640119
Ly-6G BV421	BD Biosciences	RRID:AB_2737756
I-A(b) FITC	BD Biosciences	RRID:AB_10894585
IgD(b) FITC	BD Biosciences	RRID:AB_394859

Continued

REAGENT or RESOURCE	SOURCE	IDENTIFIER
IgD AF700	BioLegend	RRID:AB_2563340
IgG AF488	Southern Biotech	RRID:AB_2794351
IgM(b) FITC	BD Biosciences	RRID:AB_396117
IgG2a-FITC	Southern Biotech	RRID:AB_2794476
Streptavidin PE/Cy7	BD Biosciences	RRID:AB_10049577
T-bet PE/Cy7	eBioscience	RRID:AB_11042699
Chemicals, peptides, and recombinant proteins		
Hep-2 slides	Bio-Rad	26101
Uristix™ Reagent Strips	Siemens	10336425
dsDNA	Sigma	D8515
ampicillin	Fisher Scientific	AC61177-0050
metronidazole	Fisher Scientific	AC210340050
neomycin	Cayman	14287
vancomycin	Cayman	15327
p-nitrophenol phosphate (PNPP) substrate	ThermoFisher	34045
creatine-D_3	Cambridge Radioisotope Lab	DLM13020.25
l-tyrosine ring-13c6	Cambridge Radioisotope Lab	CLM15420.25
L-tryptophan-2,3,3-D_3	Cambridge Radioisotope Lab	DLM5820.1
L-tyrosine Ring-$^{13}C_6$	Cambridge Radioisotope Lab	CLM71030.01
L-leucine-$^{13}C_6$	Cambridge Radioisotope Lab	CDNLM68080.25
L-phenylalanine $^{13}C_6$	Cambridge Radioisotope Lab	CLM20610.1
N-BOC-L-tert-leucine	Fisher Scientific	AC368010010
N-BOC-L-aspartic acid	Fisher Scientific	AAH62590MD
succinic acid	Fisher Scientific	AC459631000
salicylic acid D_6	Cambridge Radioisotope Lab	DLM36240.25
caffeine-D_3	Fisher Scientific	NC1800731
Critical commercial assays		
leukocyte activation cocktail	BD Biosciences	550583
Fixation/Permeabilization kit	eBioscience	00-5123-43
ProLong Gold Antifade Reagent with DAPI	Cell Signaling	8961
Experimental models: Organisms/strains		
BW1 female mice	Jackson laboratories	#100008
NZW/J female mice	Jackson laboratories	#001058
BXSB/MpJ male mice	Jackson laboratories	#000740
WYaa male mice	In house breeding	
Software and algorithms		
FlowJo V10	Tree Star	https://www.flowjo.com/solutions/flowjo/downloads
Prism 9.0	Graphpad	https://www.graphpad.com/scientific-software/prism/
ImageJ	NIH	https://imagej.nih.gov/ij/
qiime-2-2020-8	N/A	https://forum.qiime2.org/t/qiime-2-2020-8-is-now-available/16229
Greengenes 13_8	N/A	https://greengenes.secondgenome.com/
Mummichog	N/A	http://mummichog-2.appspot.com/
Others		
ACE 18-PFP 100 x 2.1 mm, 2 μm column	ACE 18-PFP 100 x 2.1 mm, 2 μm column	ACE 18-PFP 100 x 2.1 mm, 2 μm column

RESOURCE AVAILABILITY

Lead contact

Further information and requests for resources and reagents should be directed to and will be fulfilled by the lead contact, Dr. Laurence Morel (morel@uthscsa.edu).

Materials availability

This study did not generate new unique reagents.

Data and code availability

- 16S rDNA sequences and metabolomic raw data are available upon request.

- This paper does not report original code.

- Any additional information required to reanalyze the data reported in this paper is available from the lead contact upon request.

EXPERIMENTAL MODEL AND STUDY PARTICIPANT DETAILS

BWF1 female mice were purchased from the Jackson Laboratory and maintained at the University of Florida. NZW females and BXSB males were bred to produce the WYaa male progeny used in the study. All procedures were performed under protocols approved by the Institutional Animal Care and Use Committees of the University of Florida and the University of Texas Health San Antonio.

METHOD DETAILS

Study design

This study aimed to investigate the effect of 2DG treatment on the gut microbiota of lupus-prone mice and to determine whether the protective effect of 2DG on lupus pathogenesis can be transferred through the gut microbiota. We used 16S rDNA sequencing to compare the distribution of fecal microbiota communities between (NZB x NZW)F1 (BWF1) and (NZW x BXSB)F1 (WYaa) lupus-prone mice that were treated with 2DG or not starting at an age when they develop autoimmune activation. Fecal metabolites were compared between the 2DG- treated and untreated mice using LC-HRMS/MS. The protective effect of 2DG on gut microbiota was examined by serial fecal gavages from 2DG-treated mice or controls into pre-autoimmune young mice of the same strain previously treated with a cocktail of antibiotics to decrease their global bacterial content. A control group of recipients were gavaged with saline. At the end of the 2DG treatment for fecal donors, and at the end of the fecal transfers, spleen and mLN were collected for immunophenotyping by flow cytometry. Renal pathology was scored, and renal immune complex deposition and immune cells infiltrates were quantified. Autoantibodies in the serum were measured by ELISA. The distribution of fecal bacteria of the BWF1 recipient mice was also compared between groups by 16S rDNA sequencing. All experiments were conducted according to protocols approved by the University of Florida Institutional Animal Care and Usage Committee.

Mouse treatments

20-week-old BWF1 females (n = 5 per group) were treated or not with 2DG (6 mg/ml, Cayman) in drinking water for 4 weeks discontinued for 12 weeks, then retreated again at 36 weeks of age when anti-dsDNA IgG was detected in the serum of treated mice (Figure S1J). the 2DG treatment was then continued until termination to prevent reemergence of autoantibodies. Urine was tested for proteinuria every 2 weeks. Mice were sacrificed when proteinuria reached > 300 mg/dl for 2 consecutive weeks or at 46 weeks of age. These mice were used as donors for FMT in 8-week-old BWF1 mice that were pre-treated with a cocktail of antibiotics [AMNV: ampicillin metronidazole neomycin (0.05% each), and vancomycin (0.025 %)] for 2 weeks. Fresh pooled feces collected from 2DG-treated or control donors starting 4 weeks after the start of treatment were diluted in PBS (one pellet per 150 μl) and 200 μl of fecal slurry was gavaged into each recipient (n= 9 - 10 per group) 3 times a week for 26 weeks. A third cohort of age-matched AMNV-treated mice (n = 5) was gavaged with 200 μl PBS (Figure S2A). Serum was collected starting at 20 weeks of age (12 weeks after FMT started) and then biweekly until termination. A similar experimental protocol was used in which 10 - 12-week-old WYaa mice were treated continuously with 2DG or not (n = 6 - 8 per group), and FMT recipients were 5-week-old WYaa mice (n = 4 per group) pretreated with AMNV for 2 weeks, and then gavaged for

9 weeks (Figure S2B). Serum was collected from recipient mice at 11 weeks of age (6 weeks after FMT), three weeks later and at termination.

Renal pathology

Paraformaldehyde-fixed paraffin kidney sections were stained with periodic acid Schiff (PAS). The type and extent of renal lesions were evaluated using a modification of the International Society of Nephrology and the Renal Pathology Society classification of lupus nephritis and the NIH activity and chronicity indices in a blinded fashion by a pathologist (W.C.). Renal parenchymal components including glomeruli, vessels, tubules, and interstitial distributed throughout the kidney sections were evaluated. At least 100 glomeruli per kidney were evaluated for the presence of mesangial expansion, mesangial and endocapillary hypercellularity, crescents and glomerulosclerosis. The GN score was computed as the sum of the 0 – 100 results obtained for each of the 6 criteria. The extent of glomerular hyaline (immune-complex) deposits was also quantified. Acute tubular injury lesions such a tubular dilatation, epithelial attenuation and tubular casts, as well as tubular cytoplasmic PAS-positive droplets in proximal tubules were noted. The presence of IgG2a and C3 immune complexes was detected in frozen sections with FITC-tagged anti-IgG2a and anti-C3, and T cell and macrophage infiltration was detected with anti-CD3-APC and F4/80-APC, respectively, as previously described.[40]

Autoantibody measurement

For the detection of ANAs, indirect immunostaining of Hep-2 slides was performed with sera diluted 1:40 and Alexa Fluor 488–conjugated goat anti-mouse IgG as previously described.[15] Fluorescence intensity was analyzed using ImageJ. Detection of anti-dsDNA IgG was performed with sera diluted 1:100 as previously described.[41] Results were normalized to a serial dilution of pooled sera from B6.*Sle1.Sle2.Sle3* mice in which the 1:100 dilution was set at 100 units.

Gut microbiota sequence analysis

Mouse fecal samples were collected and stored at −80°C. Part of the collected fecal samples was processed for microbiota analysis. 16S rRNA libraires were constructed and sequenced as described previously.[11,42,43] Briefly, a minimal sequence depth of 44,966 2 x 300-bp reads (paired-end) per sample was obtained and processed using QIIME 2 (v2020.8). Reads were merged, quality trimmed, and clustered into operational taxonomic units at 97% sequence similarity. Taxonomy was assigned using Greengenes 13_8.

Fecal metabolomic analysis

An untargeted analysis of the fecal metabolome was conducted as previously described.[27] Briefly, fecal samples homogenized in 5 mM of ammonium formate were pre-normalized to the lowest protein concentration, and spiked with internal standards (IS) solution that consisted of creatine-D_3 (4 μg/mL), leucine-D_{10} (4 μg/mL), L-tryptophan-2,3,3-D_3 (40 μg/mL), L-tyrosine Ring-$^{13}C^6$ (4 μg/mL), L-leucine-$^{13}C^6$ (4 μg/mL), L-phenylalanine $^{13}C_6$ (4 μg/mL), N-BOC-L-tert-leucine (4 μg/ml), N-BOC-L-aspartic acid (4 μg/mL), succinic acid-2,2,3,3-D_4 (4 μg/mL), salicylic acid D_6 (4 μg/mL), and caffeine-D_3 (4 μg/mL). Metabolites were extracted by protein precipitation with a solution of 8/1/1 (v/v/v) Acetonitrile/ Methanol/ Acetone. Samples were centrifuged at 20,000 x g for 10 min at 4°C to pellet the protein. Supernatants transferred into Eppendorf tubes were dried under a gentle stream of nitrogen at 30°C. The dried extracts were re-suspended with 25 μL reconstitution solution consisting of 10 ug/mL injection standards (BOC-L-Tyrosine, BOC-L-Tryptophan and BOC-D-Phenylalanine). Resuspension was allowed at 4°C for 10-15 min then samples were centrifuged at 20,000 x g for 10 min at 4°C. Supernatants were collected into LC-vials for LC-MS analysis. Global metabolomics were performed using high-resolution mass spectrometry coupled with ultra-high performance liquid chromatography (UHPLC) analyzed in positive and negative heated electrospray ionization as previously described.[11,24,42] Separation was achieved on an ACE 18-PFP 100 x 2.1 mm, 2 μm column using a gradient with mobile phase A as 0.1% formic acid in water and mobile phase B as acetonitrile with a column temperature of 25°C. Gradient elution was ramped from 0% B to 80% B over 13.0 min at 350 μL/min, which increased to 600 μL/min between 16.80 and 17.50 min for column flush and re-equilibration. The runtime was 20.50 min and full scan at 35,000 mass resolution was acquired from 2 μL injection in positive and 4 μL injection in negative ion mode. After normalizing to total ion chromatogram, intensities were tested for group significance using unpaired Student *t*-test. Metabolites from this method were identified as they are matched with retention time and *m/z* value to a reference standard. Metabolic pathway

analysis was performed using *Mummichog* with default parameters. The pathways represented by at least 2 significant metabolites in positive or negative mode are presented.

Flow cytometry

Flow cytometry was performed on splenic and mLN cells as previously described.[16] To analyze intracellular IFN-γ and IL-17A production, cells were treated with the leukocyte activation cocktail for 4 - 5 h and fixed with the Fixation/Permeabilization kit after anti-CD4 antibody staining. Gating strategies are shown in Figures S8 and S9.

QUANTIFICATION AND STATISTICAL ANALYSIS

Statistical analyses were performed with the GraphPad Prism 9.0 software. Unless indicated, differences between groups were evaluated by one-way or two-way ANOVA with correction for multiple tests, or un-paired or paired t tests, as indicated in the figure legends. The corresponding nonparametric tests were used when the data distribution deviated from normality. Results were expressed as means $\pm$ standard deviations of the mean (SEM). The levels of statistical significance were set at *: $P < 0.05$, **: $P < 0.01$, ***: $P < 0.001$ and ****: $P < 0.0001$.